Original Article

Ultrahigh field MRI determination of water diffusion rates in *ex vivo* human lenses of different age

Thomas Stahnke[1], Tobias Lindner[2], Rudolf Guthoff[1], Oliver Stachs[1], Andreas Wree[3], Sönke Langner[4], Thoralf Niendorf[5], Niels Grabow[6], Änne Glass[7], Ebba Beller[4#], Stefan Polei[2#]

[1]Department of Ophthalmology, Rostock University Medical Center, Rostock, Germany; [2]Core Facility Multimodal Small Animal Imaging, Rostock University Medical Center, Rostock, Germany; [3]Institute of Anatomy, Rostock University Medical Center, Rostock, Germany; [4]Institute of Diagnostic and Interventional Radiology, Rostock University Medical Center, Rostock, Germany; [5]Berlin Ultrahigh Field Facility, Max-Delbrück-Center for Molecular Medicine in the Helmholtz Association, Berlin, Germany; [6]Institute of Biomedical Engineering, Rostock University Medical Center, Friedrich- Rostock, Germany; [7]Institute for Biostatistics and Informatics in Medicine and Ageing Research, Rostock University Medical Center, Rostock, Germany

[#]These authors contributed equally to this work.

Correspondence to: Thomas Stahnke, PhD. Department of Ophthalmology, Rostock University Medical Center, University of Rostock, Doberaner Straße 140, D-18057 Rostock, Germany. Email: thomas.stahnke@med.uni-rostock.de.

Background: The development of presbyopia is correlated with increased lens stiffness. To reveal structural changes with age, ultrahigh field magnetic resonance imaging (UHF-MRI) was used to analyze water diffusion in differently aged human lenses *ex vivo*.

Methods: After enucleation lens extractions were performed. Lenses were photographed, weighed, and embedded in 0.5% agarose dissolved in culture medium. UHF-MRI was conducted to analyze anatomical characteristics of the lens using T2-weighted Turbo-RARE imaging and to obtain apparent diffusion coefficients (ADC) measurements. A Gaussian fit routine was used to examine the ADC histograms.

Results: An age-dependent increase in lens wet weight, lens thickness, and lens diameter was found ($P<0.001$). T2-weighted images revealed a hyperintense lens cortex and a gradually negative gradient in signal intensity towards the nucleus. ADC histograms of the lens showed bimodal distributions (lower ADC values mainly located in the nucleus and higher ADC values mainly located in the cortex), which did not change significantly with age [βPeak1=1.96E-7 (–20E-7, 10E-7), P=0.804 or βPeak2=15.4E-7 (–10E-7, 40E-7), P=0.276; respectively].

Conclusions: Clinically relevant age dependent lens hardening is probably not correlated with ADC changes within the nucleus, which could be confirmed by further measurements.

Keywords: Ultrahigh field magnetic resonance imaging (UHF-MRI); diffusion weighted imaging; aging; human lens

Submitted Oct 06, 2020. Accepted for publication Feb 18, 2021.
doi: 10.21037/qims-20-1124
View this article at: http://dx.doi.org/10.21037/qims-20-1124

Introduction

The human lens is a structure inside the eye, which grows continuously throughout life by mitosis of lens epithelial cells in the germinative zone located in the equatorial region. In lens development epithelial cell proliferation and differentiation is triggered by fibroblast growth factors (FGF) and FGF-2 plays a key role in regulating these processes (1). The anteroposterior gradient of FGF-2

that exists between the aqueous and vitreous humour is responsible for differentiation into lens epithelial cells or lens fiber cells (1,2). Inside the surrounding capsule a permanent addition of new lens fiber cells leads to an increase in axial thickness and equatorial diameter of the lens. Older fiber cells lose their nuclei and most organelles and are subsequently packed and directed towards the center of the lens (3). The increase of lens dimensions with age results in a more elliptical lens shape and the development of two anatomic main regions: the nucleus and the cortex (4). Remodeling and cell compaction of the lens, which takes place mostly in the first 20 years of postnatal life, is adding to the complexity of lens growth and development (3).

However, the biomechanical properties of lens cortex and nucleus are different and constitute the basis for accommodation (5). The ability of the lens to change its refractive power was first described by Hermann von Helmholtz in 1855 (6) and more precisely in 1908 by Allvar Gullstrand in his work on the human crystalline lens (7) and the mechanism of intracapsular accommodation (8). It took a further 100 years before Scheimpflug imaging revealed, that changes in the sagittal lens thickness during accommodation are the result of increasing lens nucleus thickness, whereas the cortex region maintains almost a constant thickness during accommodation (3,9).

With increasing age the biomechanical characteristics of the lens cortex and the lens nucleus change (3,5). The lens becomes stiffer/harder and loses the ability to be deformed in accommodation, resulting in the loss of near vision (presbyopia). Lens deforming forces are still present with increasing age, observed by a significant activity of the ciliary muscle and its contraction under binocular stimulation of accommodation in a group of pseudophakic subjects, which supports the lenticular-based theory of presbyopia in the aging eye (10-12). The reasons for the obvious nuclear hardening with age are not fully understood. Changes in crystallin composition (13), crystallin aggregate formation (14), lens fiber membrane cholesterol composition (13), decreasing water content (15), UV impairment (16), and oxidative stress (17) have been discussed in this context.

In recent years *in vivo* imaging techniques like magnetic resonance imaging (MRI) have become a common method for the visualization of the eye including the lens and the orbit (18-20). Due to its non-invasive nature, MRI allows further insights in the aging human crystalline lens anatomy, and its inner architecture during accommodation (21,22). In a comparative study of Scheimpflug photography and MRI of human lenses *in vivo* a good agreement of generated data was shown (23). Several MRI techniques like T1-, T2-, and proton density weighted imaging allow differentiated visualization of ocular structures and a distinction between specific tissues based on their compositions and water contents (24). Several studies investigated the crystalline lens using diffusion-weighted magnet resonance imaging (DWI-MRI), which measures the rate of diffusion of water molecules within a tissue. For example, an increase in T2 relaxation time and water diffusion was measured in lenses of diabetic versus healthy rabbits *in vivo* detected by DWI-MRI at 4.7 T (25).

Further developments of DWI-MRI, resulted in diffusion tensor magnetic resonance imaging (DT-MRI), which gives additionally information about the orientation and quantitative anisotropy of the water diffusion (26). In bovine lenses *ex vivo* diffusion tensor magnetic resonance imaging (DT-MRI) at 4.7 T revealed novel anisotropic polar and equatorial zones of pronounced diffusivity directed transverse to the fiber cells, whereas an inner zone (including the lens nucleus) showed isotropic and weak diffusivity (27,28). DT-MRI measurements at 9.4 T of bovine lenses *ex vivo* demonstrated a sharp boundary in fractional anisotropy between the outer cortex and inner nucleus of the lens with highest anisotropy measured in the lens nucleus (29). However, DWI-MRI and/or DT-MRI data in human lenses of different ages are limited. Moffat and Pope examined human lenses of different age *ex vivo* using DT-MRI at 4.7 T (30). They demonstrated that diffusion parallel to the long axes of the fiber cells is relatively unrestricted, whereas diffusion perpendicular to the cells is inhibited by the cell membranes, particularly in the inner cortex region of the lens, confirming the presence of a diffusion barrier surrounding the lens nucleus (30).

Improvements in image resolution together with the introduction of enhanced DWI-MRI mapping techniques in ophthalmic examinations was demonstrated by Paul *et al.* using magnetic field strengths of 3.0 T, 7.0 T, and 9.4 T (31,32). Ultrahigh field (UHF-MRI), and extreme field MRI (EF-MRI) at 20 Tesla and beyond were recommended to boost spatial resolution and close the wide gap between the view of biologists and clinicians (33).

Recognizing the sensitivity gain, spatial resolution enhancement and progress in diffusion mapping techniques, UHF-MRI is conceptually appealing for the study of an age dependent lens hardening and water diffusion rates within the lens. Detailing and understanding this correlation may provide further insights into the biomechanical behavior

of the human lens and the onset of presbyopia. With this rationale in mind the present study focuses on the *ex vivo* assessment of human lenses of different age with UHF-MRI at 7.0 T. To meet this goal, T2-weighted Turbo-rapid acquisition with relaxation enhancement (RARE) imaging was conducted to analyze anatomical characteristics. For the assessment of the apparent diffusion coefficient (ADC) of water in the lens, diffusion sensitized spin-echo techniques were employed.

Methods

Ethical consent

The authors are accountable for all aspects of the work in ensuring that questions related to the accuracy or integrity of any part of the work are appropriately investigated and resolved. This study was approved by the ethics committee of the Rostock University Medical Center (approval ID: A 2015-0009) and followed the guidelines of the Declaration of Helsinki (as revised in 2013). Written informed consent was obtained from all patients before donation.

Human material

Differently aged human lenses ranging from the age of 31 to the age of 89 years were received from 117 human cadavers without known eye disease. The donor eyes were transported to the laboratory in sealed containers and stored at 4 ℃ before use. Depending on the limited UHF-MRI scan time availability 45 lenses were analyzed by UHF-MRI over night to examine anatomical characteristics and evaluated upon the specific donor age. Due to the long measurement protocol for DWI, only 32 lenses were scanned with the DWI protocol. For data analysis, ADCs were evaluated based upon the specific donor age.

Lens preparation

Immediately after enucleation intracapsular lens extraction was performed. Lenses were transferred into 0.9 % NaCl-solution (B. Braun Melsungen AG, Melsungen, Germany), photographed, and weighed (n=117). Within 24 hours of passing 45 lenses were embedded in cooled 0.5 % agarose (peq GOLD, # 35-1020, VWR International GmbH, Darmstadt, Germany) solved in culture medium (# F9016, BIOCHROM GmbH, Berlin, Germany) into a 15 ml tube for UHF-MRI examinations (n=45). All experiments were replicated in the same manner.

UHF-MRI examination

UHF-MRI (7.0 Tesla, BioSpec 70/30, gradient insert: BGA-12S, maximum gradient strength: 440 mT/m, RF coil: two element array, cryogenic ^{1}H transmit/receive RF surface coil with 23 mm in diameter, software interface: Paravision 6.0.1, Bruker, Ettlingen, Germany) was conducted to analyze anatomical characteristics, axial thickness, and equatorial lens diameter in the central layer of each lens using T2-weighted Turbo-RARE sequences (Rapid Acquisition with Relaxation Enhancement) for axial and coronal slices (TE/TR: 51/5,500 ms, matrix size: 162×205 (axial) and 172×210 (coronal), FoV approx.: 12 mm×15.5 mm (axial) and 13 mm ×16 mm (coronal), in plane spatial resolution: 75 µm×75 µm, slice thickness: 800 µm, scan time: 1 h 22 min).

2D multi-slice spin-echo based diffusion imaging (6 non-collinear and non-planar diffusion directions, 5 b-values (0, 100, 350, 700, 1,000) s/mm^2, TE/TR: 22/3,000 ms, matrix: 153×206, FoV: 15.5×20.5 mm, in plane spatial resolution: 100 µm×100 µm, slice thickness: 800 µm, scan time: 15 h 45 min) was conducted for ADC mapping in 32 lenses. The ADC map (derived from all b-values) was generated using the standard scanner software (Image-Sequence-Analysis-Tool), which is part of the Image Display and Processing tool of the Paravision 6.01. software. The fitting function dtraceb of the Image-Sequence-Analysis-Tool uses the b-values calculated from the protocol parameters and is based on the magnitude images of the reconstructed dataset. All diffusion experiments were carried out with the cryo-cooled RF coil heating system set to 35 ℃, which had no direct contact to the tube containing the lens. This led to a measured sample temperature of 30 ℃. The temperature was maintained during the whole experiment.

Image analysis

After slice wise separation of lens and culture medium by free hand drawn region of interests (ROI), histograms were generated for each multi slice ADC data set. In all lenses examined resulting histograms exhibited two distinct peaks: one peak with mean ADC-values of $(0.5\pm0.1)\times10^{-3}$ mm^2/s, and another peak at higher ADCs around $(0.7\pm0.1)\times10^{-3}$ mm^2/s ($P<0.001$; see *Figure 1* for histograms of two different aged lenses). Based on this observation we assumed that the ADC-value has a bimodal distribution. Thus, to determine peak positions the histograms of individual lenses were fitted with a double Gaussian peak function. Fitted peak positions for the two modes were plotted against lens ages. Segmentation and the following computational steps

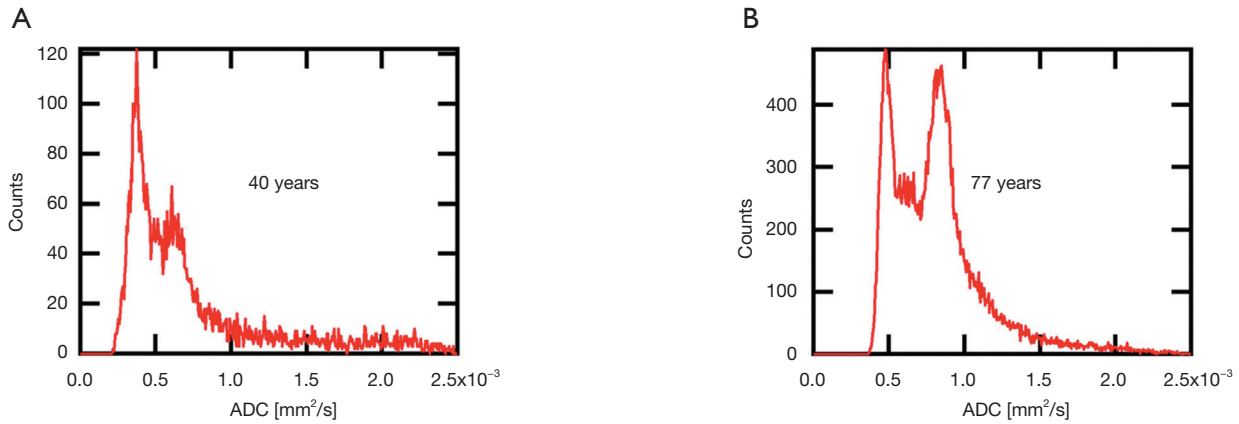

Figure 1 Bimodal distribution of peak positions in ADC histograms. Exemplarily, histograms of 2 human lenses are shown. (A) 40 years old lens; (B) 77 years old lens. ADC, apparent diffusion coefficients.

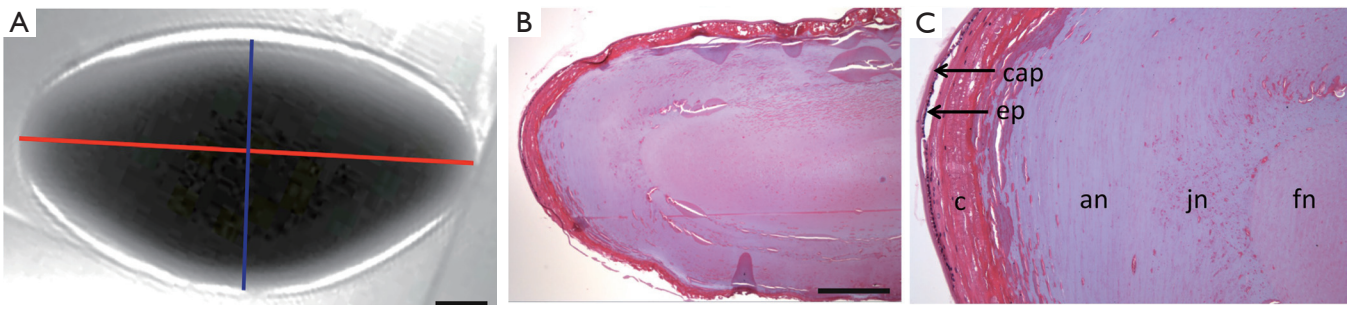

Figure 2 MRI and histology of a representative human lens (58 years). In T2-weighted images, lens measurements were performed manually of equatorial diameter (red line) and axial thickness (blue line). It can also be noticed that the lens cortex area appears hyperintense and signal intensity decreases gradually towards the nucleus (A). Histological examination revealed comparable differences in the inner architecture of the lens (B). Lens capsule (cap), epithelium (ep), cortex (c), adult nucleus (an), juvenile nucleus (jn) and fetal nucleus (fn) can be identified at 10× magnification (C). HE stain; bars: 1 mm.

were performed with the Igor Pro software package (V. 6.37, WaveMetrics Inc., Lake Oswego, USA).

Lens geometry was measured by using the Paravision 6.01. software of the scanner. T2w images were visually screened for the largest cross section area. The following length measurements of the respective slice were then performed manually: Equatorial diameter (ED; 6 to 12 o'clock axis of the lens) and axial lens thickness (AT; from anterior to posterior pole) of the crystalline lens with AT being perpendicular to ED (*Figure 2*).

Histology

Following UHF-MRI lenses were embedded in paraffin. Histological sections of 5 µm thickness were hematoxylin-eosin (H&E) stained using a standard protocol (34). Shortly, after dewaxing in xylene, sections were hydrated in decreasing percentages of alcohol and stained with hematoxylin (Merck Millipore, Darmstadt, Germany). Thereafter, sections were dehydrated in increasing percentages of alcohol until 70% and stained with 1% eosin G (Merck Millipore). Differentiation occurred in 90% alcohol, followed by clearing in xylene, and finally mounting in Entellan® (Merck Millipore).

Statistical analysis

All data were processed using IBM® Advanced Statistics SPSS® 24.0. Values are expressed as mean ± standard deviation (SD) for the indicated number of samples. Linear

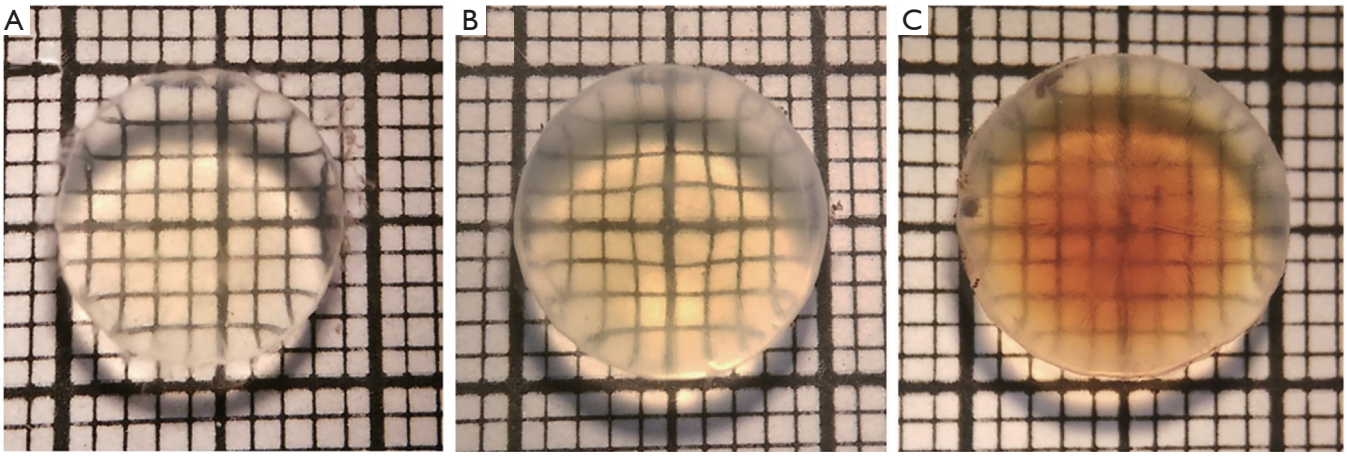

Figure 3 Isolated human lenses. Three differently aged human lenses with early signs of opacification (B, C) and increasing lens yellowing (A to C) are shown. (A) 34 years old lens; (B) 62 years old lens; (C) 87 years old lens.

Regression analyses were performed to evidence the influence of age on weight, thickness, diameter, and ADC of lenses. Slopes (β) of regression with their respecting 95% confidence intervals (95% CI) as well as P values for testing β=0 are given.

The datasets generated and analyzed during the current study are available from the corresponding author upon reasonable written request.

Results

Assessment of lens size and transparency

Dissected donor lenses of different ages were examined under a microscope and photographed (*Figure 3*). It was obvious that lens diameters increased with age. With increasing donor age also lens color changed from faint to dark yellow, which reached a light brown in the oldest lenses.

Wet weight and UHF-MRI examinations

Before embedding the donor lenses for UHF-MRI examinations, the wet weight of each lens was determined. Lens wet weight increased with age from 0.197±0.010 g for the youngest lenses (31 years, n=2) to 0.289±0.042 g for the oldest lenses (89 years, n=4) significantly (slope =1.594±0.1506 mg increase per year; P<0.001, *Figure 4A*).

UHF-MRI examinations using T2-weighted Turbo-RARE sequences were conducted to determine the axial lens thicknesses (*Figure 4B*) and equatorial lens diameters (*Figure 4C*) in the central layer of each lens. The mean axial lens thickness for youngest lens (31 years, n=1) was 4.79 mm and increased with age to 5.58 mm measured in the lens of the oldest donor (89 years, n=1) (P<0.001). The mean equatorial lens diameter increased from 8.87 mm in the youngest lens (31 years) to 10.19 mm (89 years) (P<0.001).

In T2-weighted images lens capsules appeared hypointense, the underlying hyperintense layer represents the outer cortical region. This hyperintense area is less visible in the equatorial region, where consistent signal intensity was observed, which was also present in the remaining lens cortex. The lens cortex could be differentiated from the nucleus region, which was characterized by a more hypointense signal. Lens capsules, hyperintense cortical regions, lens cortices and lens nuclei showed a gradually change in signal intensity (*Figure 2A*). These hyperintense areas are also described in the literature by Stahnke *et al.* (35).

Histological analyzes of H&E stained human lenses also clearly demonstrated differences in lens organization (*Figure 2B,C*). Beneath the lens capsule the monolayered lens epithelium was obvious in the anterior part of the lens. The outer lens cortex appeared red stained, followed by a sharply separated, bluish stained area, and another defined nuclear region, which was stained faint red. These results seem to be similar with the findings obtained from T2-weighted UHF-MRI examinations, where the lens cortex area appeared hyperintense and signal intensity decreases gradually towards the nucleus (*Figure 2A*).

ADC values, determined with DWI-MRI examinations,

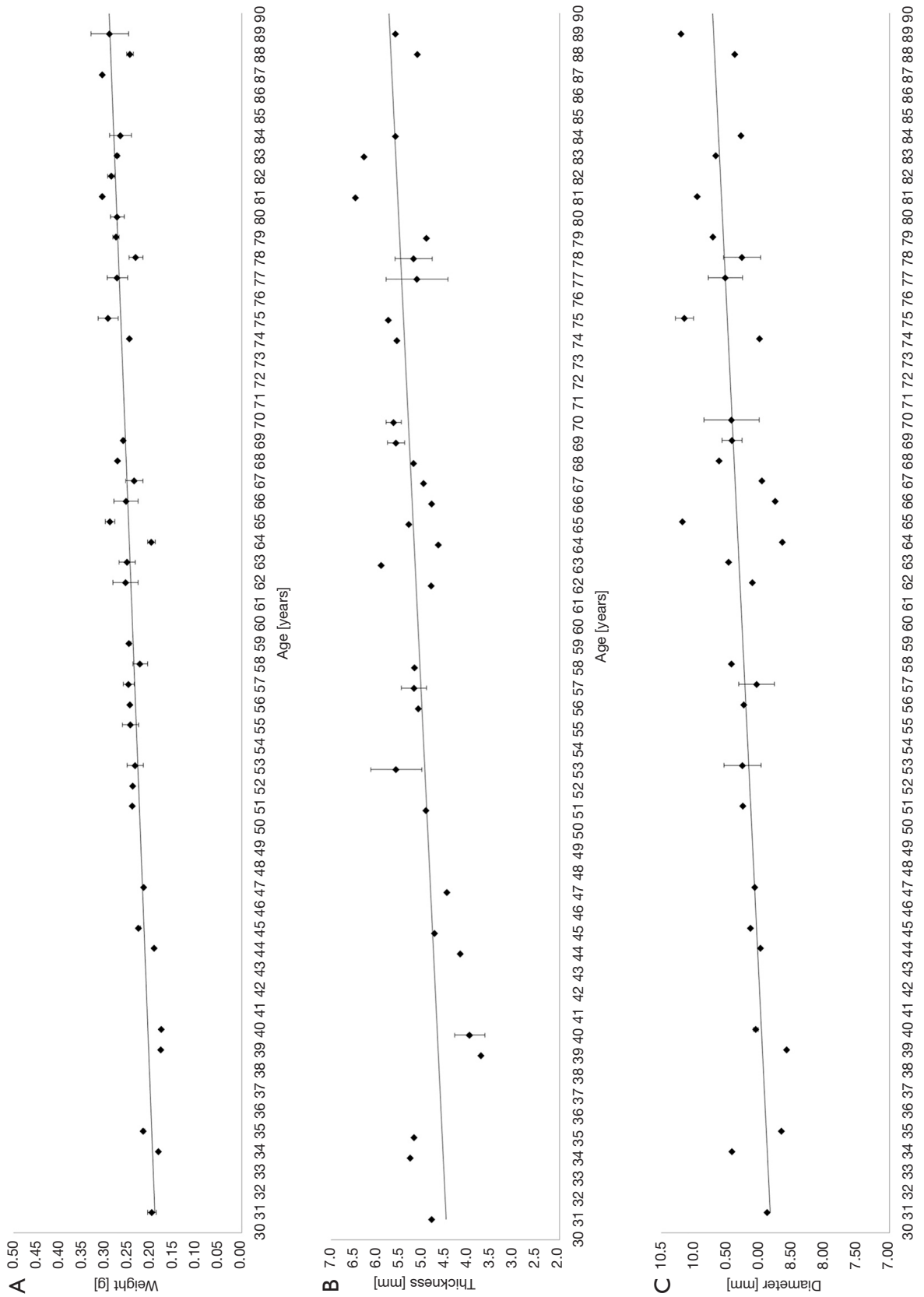

Figure 4 Wet weight, axial thickness, and equatorial diameter of human lenses of different ages. (A) An age-dependent increase in lens wet weight could be detected by regression ($weight_{mg}$ =0.00162 age_{ys} + 0.143; P_β<0.001). (B) In T2-weighted images an increase in axial lens thickness ($thickness_{mm}$ =0.020 age_{ys} + 3.85; P_β<0.001) and (C) equatorial lens diameter ($diameter_{mm}$ =0.0148 age_{ys} + 8.36; P_β<0.001), influenced by age was determined. Error bars correspond to standard deviation.

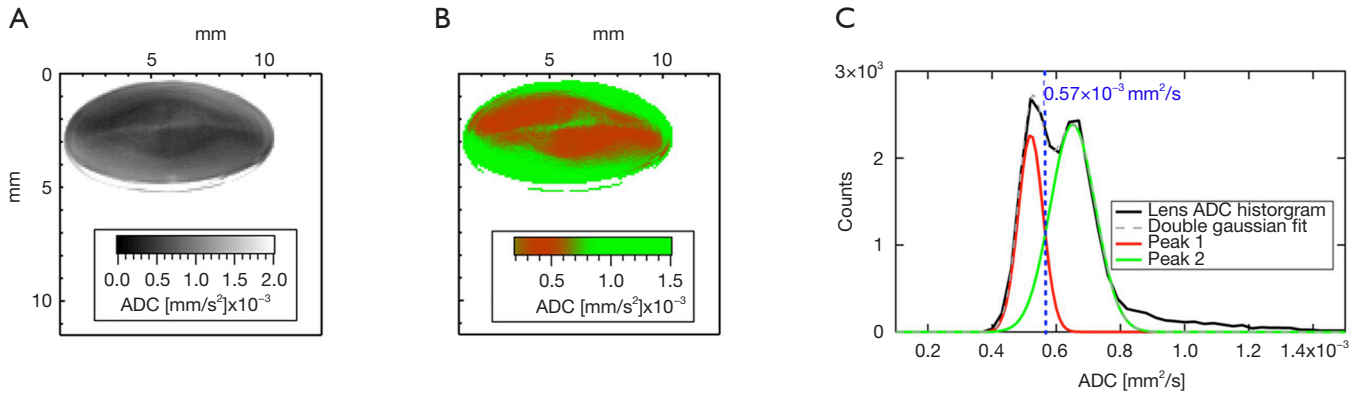

Figure 5 Distribution and evaluation of ADC values in an example lens (67 years). ADC map shows ADC value of an *ex vivo* human lens plotted pixel wise (A) and with color coded representation (B). Histogram analysis of the ADC values of the lens shows bimodal ADC distribution. According to the height ratios of the two Gaussian peaks (Peak 1 and Peak 2) at a certain ADC value, a mixed color is computed pixel wise (dashed line represents a 50% red and 50% green distribution). In conjunction with the local arrangement of ADC values, the results indicate that the first mode represents mainly the lens nucleus, whereas the cortex region is primarily represented by the second mode (C). ADC, apparent diffusion coefficients.

displayed a bimodal distribution within the lenses (*Figure 5*). Using a gradient color scale (from red to green) adopted to the distribution of the lens ADC values (*Figure 5A*), the local occurrence of areas with different ADC values within the lens can be visualized (*Figure 5B*). For each ADC-value a mixed color corresponding to the relative height of the two fitted Gaussian peaks at a given ADC value (e.g., at 0.57 mm^2/s 50% red and 50% green (*Figure 5C*, dashed line) resulting in a reddish-brown tone, which is visualized in the color scale in *Figure 5B*) was computed. The results showed that the first mode (lower ADC values) represents mainly diffusion within the lens nucleus, whereas the second mode represents diffusion in the cortex region (*Figure 5B*).

Peak positions of the first mode in the ADC histogram appear to remain essentially constant (~0.5×10^{-3} mm^2/s) with increasing lens age, reflected by a regression coefficient not different from zero [β_{Peak1}=1.96E-7 (–20E-7, 10E-7], P=0.804]. The second mode peak position seems to tend towards higher values with increasing age, but could not be evidenced by regression analysis [β_{Peak2}=15.4E-7 (–10E-7, 40E-7), P=0.276; *Figure 6*].

Discussion

The mechanical properties of the human crystalline lens, which are responsible for the ability of the lens to change its shape during accommodation, are changing with age (36). These changes are thought to have an effect on the accommodative ability and the development of presbyopia, which is a condition inherent to normal aging (37).

Reasons for the appearance of presbyopia are still unknown; the correlation with permanent lens growth throughout life has been discussed in this context (3,38,39). In our study we examined lens growth by determination of the lens wet weight and axial as well as equatorial lens dimensions derived from T2-weighted MRI at 7.0 T. An increase in lens wet weight with age was observed, which confirms the permanent growth of a lens with age. We also observed an increased appearance of lens yellowing with age up to a light brown in the oldest lenses. These findings were already described and caused by accumulation of the fluorogen glutathione-3-hydroxy kynurenine glycoside (40,41). Axial lens thickness and equatorial lens diameters of isolated human lenses increased with age in our examinations. It has to be considered, that the lens diameter from isolated lenses does not represent its diameter in the living eye. During lens dissection the zonular fibers were cut and young lenses underwent a fully accommodative process leading to a decrease in lens diameter, whereas the older, presbyopic and stiff lenses did not (42). The measured increase in equatorial lens diameter with age in presbyopic lenses (between 60–90 years) led to the assumption, that lifetime lens growth also results in an increase of this parameter, because presbyopic lenses do not have the ability to accommodate anymore. These findings do not correspond with a MRI based study, which demonstrated

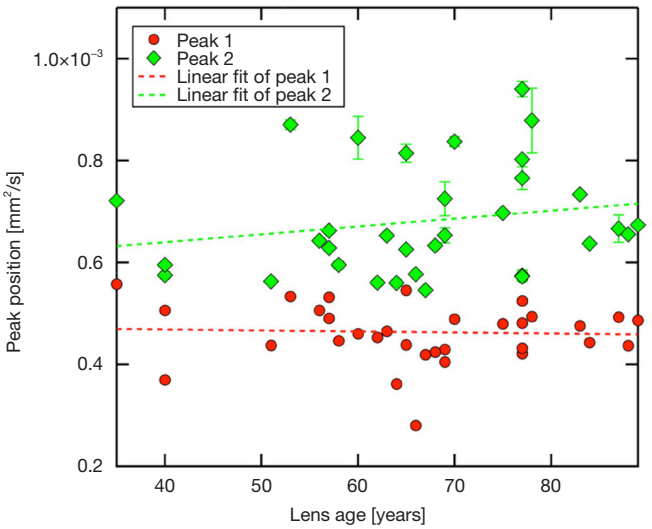

Figure 6 ADC-values of differently aged lenses. Age-dependence of the peak positions of the two ADC histogram modes. Error bars correspond to estimated error (standard deviation) as derived from the double Gaussian fit. ADC values of the first mode appear to remain constantly with age ($ADC_{mm2/s}$ = 1.96E-7 Age_{ys} + 0.476E-3; P_{β}=0.804). With increasing age, peak positions of the second mode seem to tend towards higher ADC values, but this is not evidenced ($ADC_{mm2/s}$ = 15.4E-7 Age_{ys} + 0.578E-3; P_{β}=0.276). Regression lines (dotted) show different slopes for both groups Peak 1 and 2 (n=32 each).

a consistent equatorial lens diameter with increasing age *in vivo* (18,43), but are in line with several studies demonstrating an increase of equatorial lens diameter *in vitro* (3,44) and *in vivo* (45,46).

Lens stiffening as cause for presbyopia by the lifelong addition of cellular material is still in the focus of research (3), but the knowledge about the stiffness distribution within the lens is limited (47). It has been observed, that lens stiffness is lowest near the center of the nucleus and increases towards the periphery of the cortex in younger human lenses, whereas the center of the nucleus is stiffer than the periphery of the cortex in older lenses (36). Similar results have been demonstrated by Heys *et al.*, who reported that the nucleus gets stiffer than the cortex between 35–40 years in humans (5). Using a coaligned ultrasound and optical coherence elastography system Wu *et al.* observed that the maximum displacements of young rabbit lenses were significantly larger than those of mature lenses, indicating a gradual increase of the lens stiffness with age (48). This gradual age-related stiffening of the lens is probably the primary reason for presbyopia and associated with gradual age-related loss of accommodation (37,42).

The development of presbyopia was also examined by *in vivo* visualization of lenses during accommodation using MRI at 1.5 Tesla (17,49). Since then, image quality of MRI examinations has been improved significantly due to the application of higher magnetic field strengths and the availability of RF coil technology tailored for eye imaging (21). These developments led to an increase in the signal-to-noise ratio (SNR), which increased image resolution nearly to a microscopic level for detailed anatomical examinations (35,50). In this study we used UHF-MRI at 7 Tesla to analyze anatomical characteristics of the human lens. We observed a gradually decrease in T2-weighted signal intensity from the lens cortex towards the lens nucleus. Using histological staining methods distinct separated areas within the lens were detected confirming our UHF-MRI findings. The decrease of signal intensity from the lens cortex to the lens nucleus is caused by changes in the water/-protein ratio of the lens. In previous studies it has been described that water content is highest in the cortex of the lens and lowest in the central nucleus (51,52). Higher protein content causes a reduction in water molecules, resulting in a lower concentration of protons responsible for the MRI signal. To verify this phenomenon we measured aqueous bovine serum albumin (BSA) solutions in increasing concentrations resulting in a decrease in T2-weighted signal intensity with increasing protein concentrations, which was also previously described by Yilmaz *et al.* (53).

Due to the fact that the main changes that occur with aging in the lens are reduced diffusion of water from its cortical to its nuclear zone (54) we analyzed the behavior of water inside different lens areas measuring its diffusion to gain more insights into lens architecture and to detail the influence of aging. Using DWI-MRI, which is sensitive to the diffusion of water molecules and probes their random displacement within tissues, it is possible to identify areas of different (isotropic or anisotropic) water diffusion behavior in the lens. DWI-MRI is of proven value for an ever-growing range of clinical indications and provides qualitative and quantitative information for tissue characterization (24). Recognizing the capabilities of DWI-MRI we hypothesized, like Vaghefi *et al.* (28), and Moffat & Pope (30), that diffusion rates differ in specific lens areas with a different compaction or stiffness degree and that it is possible to visualize these changes by UHF-MRI ADC measurements. Also, Wu *et al.* demonstrated different

anisotropic diffusion patterns and diffusion coefficients in lens cortex and nucleus regions in a rabbit cataract model (55). In contrast to their examinations, we performed our measurements on a higher number of human lenses and at higher magnetic field strength of 7 Tesla.

To establish a protocol for MRI based diffusion coefficient calculations of bovine lenses Vaghefi *et al.* evaluated the influence of different b-values on image quality (28). They demonstrated a slight attenuation of signal intensity with increasing b-values, and significant blurring artifacts at higher b-values (>1,620 s/mm^2), possibly due to vibration induced by rapid switching of large magnetic field gradients. These artifacts were not observed in our study. However, to address the possible influence of higher b-values, we analyzed ADC data for three randomly selected lenses with b-values of 4,000 s/mm^2 (data not shown). The corresponding bimodal fit revealed similar results as the ADC investigation with b-values of 1,000 s/mm^2, concluding no significant difference between lens measurements with b-values of 1,000 s/mm^2 and 4,000 s/mm^2.

Our investigations concerning diffusion rates raise the question as to whether or not ADC-values are in fact dependent on donor age of human lenses. Data shown in *Figure 6* might indicate an increase of ADC in the cortex region with increasing age, whereas regression analysis did not evidence this. ADC-values mainly representing the nucleus region seem to remain steady over time. They are lower than on the cortex level. The question on possible age-dependence of ADC-values in cortex region *vs.* a longitudinal stability of diffusion in the center of the lens remains to be clarified, potentially by powering the study fourfold. Furthermore, the map of ADC values did not appear to be strictly restricted to either the cortex or the nucleus. This could mean that a peripheral fibre cell stretching from pole to pole could be passing through different regions of ADC values. Since in diffusion-weighted imaging the overwhelming portion of the signal is obtained from the extracellular diffusion of water molecules (56), this could be interpreted as different diffusion rates of the extracellular space for the same cell. However, further analysis is required, probably at a cellular level.

An age-dependence of diffusion rates in human lenses was described by Moffat *et al.*, who observed a decrease in transport rates into the nucleus and the forming of a diffusion barrier with age (57). He concluded that this diffusion barrier could lead to longer lifetimes of reactive species within the lens and to a slower rate at which anti-oxidants could enter the nucleus, contributing to increased damage to lens crystallins as a potential reason for presbyopia in older lenses. Taken into consideration that lens nutrition is based on diffusion of aqueous humor and its own internal microcirculatory system, which is faster than the passive diffusion alone (58), an involvement of active mechanisms inside the lens is obvious. The microcirculatory system is primarily ion (Na^+) driven realized by sodium pumps (Na^+/K^+-ATPase) using the extracellular space to reach nuclear regions (58,59) changing to a gap junction mediated intercellular pathway directed to the lens periphery (59). Interestingly, the gap junctions differ between lens fiber cells in the nucleus and cortical lens fibers (60,61) leading to the assumption that intercellular fluid flow is different in nuclear and cortical regions. Moreover, the gap junction protein MP70, which is mainly localized in the lens cortex region, is proteolyzed in an age-dependent manner (62). The lipid-to-protein weight ratio as well as the total lipid composition of fiber cell plasma membranes is altered chemically in the cortex and the nucleus with age (62). However, whether these age-dependent modifications in the internal microcirculatory system of the lens, which could lead to changes in the diffusion of the extracellular space, may explain the findings described by Moffat *et al.* (57) and our own observations of different diffusion values in the lens cortex and the lens nucleus, remain highly speculative. Nevertheless, our results do not indicate a connection between the clinically observable and in literature described hardening of the nucleus with age (5) and ADC, which seems to be constant with age in lens nucleus.

Limitations

Our study has several limitations worth noting. For the second mode peak position, representing mainly the cortex, we observed a greater variance of the ADC values compared to the first mode peak position. This could potentially be due to the differences in processing time of the lenses, which was only limited to 24 hours, unknown lens pathologies or the experimental technique, e.g., damage to the cortex during lens extraction or preparation and water accumulation between the lens and agarose (*Figure 2*) likely due to shrinkage, which might lead to water evaporating from the lens cortex. However, the water accumulation between lens and agarose described above was not included in the analysis. Furthermore, we cannot rule out that the solutions, in which the enucleated lenses were

preserved, did not affect the T2 signal intensity as shown by Vaghefi *et al.* in enucleated bovine lenses (63). In this study no T1-weighted images of the lens were acquired, which could have been helpful in determining whether the decrease in T2 signal intensity of the lens nucleus is due to increased protein content. Finally, we used the same TE for ADC measurements of lens cortex and nucleus, however short TEs are recommended for T2-weighted-imaging of the nucleus and could therefore affect the ADC measurements (19).

Conclusions

Detailed anatomical characteristics and diffusion coefficients of human lenses can be visualized by UHF-MRI *ex vivo* as shown in this study, which is more powerful than existing studies on human lenses with a greater sample size, examined at ultrahigh magnetic field strength (7T). It was demonstrated that apparent water diffusion coefficients differ between the cortex region and the nucleus. However, age dependence of ADC values remains to be clarified. To ascertain that the clinically observed age related hardening of the lens is not reflected in a change of water diffusion in the nucleus, further measurements are necessary.

Acknowledgments

The authors appreciate the excellent laboratory work of Colette Leyh. Financial support by the Federal Ministry of Education and Research within RESPONSE "Partnership for Innovation in Implant Technology" is gratefully acknowledged.
Funding: None.

Footnote

Conflicts of Interest: All authors have completed the ICMJE uniform disclosure form (available at http://dx.doi.org/10.21037/qims-20-1124). Dr. TN reports other from MRI.TOOLS GmbH, Berlin, Germany, outside the submitted work. The other authors have no conflicts of interest to declare.

Ethical Statement: This study was approved by the ethics committee of the Rostock University Medical Center (approval ID: A 2015-0009) and followed the guidelines of the Declaration of Helsinki (as revised in 2013). Written informed consent was obtained from all patients before donation.

References

1. Wu W, Tholozan FM, Goldberg MW, Bowen L, Wu J, Quinlan RA. A gradient of matrix-bound FGF-2 and perlecan is available to lens epithelial cells. Exp Eye Res 2014;120:10-4.
2. DiVittorio R, Bluth EI, Sullivan MA. Deep Vein Thrombosis: Diagnosis of a Comon Clinical Problem. Ochsner J 2002;4:14-7.
3. Augusteyn RC. On the growth and internal structure of the human lens. Exp Eye Res 2010;90:643-54.
4. Dubbelman M, Van der Heijde GL, Weeber HA, Vrensen GF. Changes in the internal structure of the human crystalline lens with age and accommodation. Vision Res 2003;43:2363-75.
5. Heys KR, Cram SL, Truscott RJ. Massive increase in the stiffness of the human lens nucleus with age: the basis for presbyopia? Mol Vis 2004;10:956-63.
6. Cate-Hoek AJt. Prevention and treatment of the post-thrombotic syndrome. Research and Practice in Thrombosis and Haemostasis 2018;2:209-19.
7. Caronia J, Sarzynski A, Tofighi B, Mahdavi R, Allred C, Panagopoulos G, Mina B. Resident performed two-point compression ultrasound is inadequate for diagnosis of deep vein thrombosis in the critically III. J Thromb Thrombolysis 2014;37:298-302.
8. Cabrera R, Chimalakonda N, Rosario J, Ganti L. The Role of Serial Ultrasounds in Diagnosing Suspected Deep Venous Thrombosis. Cureus 2019;11:e4337.
9. Koretz JF, Cook CA, Kaufman PL. Accommodation and presbyopia in the human eye. Changes in the anterior segment and crystalline lens with focus. Invest Ophthalmol Vis Sci 1997;38:569-78.
10. Özyol E, Özyol P. Evaluating relaxed ciliary muscle tone

in presbyopic eyes. Graefes Arch Clin Exp Ophthalmol 2017;255:973-8.
11. Stachs O, Martin H, Kirchhoff A, Stave J, Terwee T, Guthoff R. Monitoring accommodative ciliary muscle function using three-dimensional ultrasound. Graefes Arch Clin Exp Ophthalmol 2002;240:906-12.
12. Tabernero J, Chirre E, Hervella L, Prieto P, Artal P. The accommodative ciliary muscle function is preserved in older humans. Sci Rep 2016;6:25551.
13. Bron AJ, Vrensen GF, Koretz J, Maraini G, Harding JJ. The ageing lens. Ophthalmologica 2000;214:86-104.
14. Boyle D, Takemoto L. Characterization of the alpha-gamma and alpha-beta complex: evidence for an in vivo functional role of alpha-crystallin as a molecular chaperone. Exp Eye Res 1994;58:9-15.
15. Siebinga I, Vrensen GF, De Mul FF, Greve J. Age-related changes in local water and protein content of human eye lenses measured by Raman microspectroscopy. Exp Eye Res 1991;53:233-9.
16. Roberts JE. Ultraviolet radiation as a risk factor for cataract and macular degeneration. Eye Contact Lens 2011;37:246-9.
17. Michael R, Bron AJ. The ageing lens and cataract: a model of normal and pathological ageing. Philos Trans R Soc Lond B Biol Sci 2011;366:1278-92.
18. Strenk SA, Semmlow JL, Strenk LM, Munoz P, Gronlund-Jacob J, DeMarco JK. Age-related changes in human ciliary muscle and lens: a magnetic resonance imaging study. Invest Ophthalmol Vis Sci 1999;40:1162-9.
19. Muir ER, Pan X, Donaldson PJ, Vaghefi E, Jiang Z, Sellitto C, White TW. Multi-parametric MRI of the physiology and optics of the in-vivo mouse lens. Magn Reson Imaging 2020;70:145-54.
20. Streckenbach F, Klose R, Langner S, Langner I, Frank M, Wree A, Neumann AM, Glass Ä, Stahnke T, Guthoff RF, Stachs O, Lindner T. Ultrahigh-Field Quantitative MR Microscopy of the Chicken Eye In Vivo Throughout the In Ovo Period. Mol Imaging Biol 2019;21:78-85.
21. Langner S, Martin H, Terwee T, Koopmans SA, Krüger PC, Hosten N, Schmitz KP, Guthoff RF, Stachs O. 7.1 T MRI to assess the anterior segment of the eye. Invest Ophthalmol Vis Sci 2010;51:6575-81.
22. Graessl A, Muhle M, Schwerter M, Rieger J, Oezerdem C, Santoro D, Lysiak D, Winter L, Hezel F, Waiczies S, Guthoff RF, Falke K, Hosten N, Hadlich S, Krueger PC, Langner S, Stachs O, Niendorf T. Ophthalmic magnetic resonance imaging at 7 T using a 6-channel transceiver radiofrequency coil array in healthy subjects and patients with intraocular masses. Invest Radiol 2014;49:260-70.
23. Koretz JE, Strenk SA, Strenk LM, Semmlow JL. Scheimpflug and high-resolution magnetic resonance imaging of the anterior segment: a comparative study. J Opt Soc Am A Opt Image Sci Vis 2004;21:346-54.
24. Lindner T, Langner S, Paul K, Pohlmann A, Hadlich S, Niendorf T, Jünemann A, Guthoff RF, Stachs O. Diffusion Weighted Magnetic Resonance Imaging and its Application in Ophthalmology. Klin Monbl Augenheilkd 2015;232:1386-91.
25. Cheng HM. Water diffusion in the rabbit lens in vivo. Dev Ophthalmol 2002;35:169-75.
26. Soares JM, Marques P, Alves V, Sousa N. A hitchhiker's guide to diffusion tensor imaging. Front Neurosci 2013;7:31.
27. Vaghefi E, Pontre B, Donaldson PJ, Hunter PJ, Jacobs MD. Visualization of transverse diffusion paths across fiber cells of the ocular lens by small animal MRI. Physiol Meas 2009;30:1061-73.
28. Vaghefi E, Donaldson PJ. An exploration into diffusion tensor imaging in the bovine ocular lens. Front Physiol 2013;4:33.
29. Ho LC, Sigal IA, Jan NJ, Yang X, van der Merwe Y, Yu Y, Chau Y, Leung CK, Conner IP, Jin T, Wu EX, Kim SG, Wollstein G, Schuman JS, Chan KC. Non-invasive MRI Assessments of Tissue Microstructures and Macromolecules in the Eye upon Biomechanical or Biochemical Modulation. Sci Rep 2016;6:32080.
30. Moffat BA, Pope JM. Anisotropic water transport in the human eye lens studied by diffusion tensor NMR micro-imaging. Exp Eye Res 2002;74:677-87.
31. Paul K, Huelnhagen T, Oberacker E, Wenz D, Kuehne A, Waiczies H, Schmitter S, Stachs O, Niendorf T. Multiband diffusion-weighted MRI of the eye and orbit free of geometric distortions using a RARE-EPI hybrid. NMR Biomed 2018. doi: 10.1002/nbm.3872.
32. Paul K, Graessl A, Rieger J, Lysiak D, Huelnhagen T, Winter L, Heidemann R, Lindner T, Hadlich S, Zimpfer A, Pohlmann A, Endemann B, Krüger PC, Langner S, Stachs O, Niendorf T. Diffusion-sensitized ophthalmic magnetic resonance imaging free of geometric distortion at 3.0 and 7.0 T: a feasibility study in healthy subjects and patients with intraocular masses. Invest Radiol 2015;50:309-21.
33. Niendorf T, Barth M, Kober F, Trattnig S. From ultrahigh to extreme field magnetic resonance: where physics, biology and medicine meet. Magma 2016;29:309-11.
34. Fisher RF, Pettet BE. Presbyopia and the water content of the human crystalline lens. J Physiol 1973;234:443-7.

35. Stahnke T, Hadlich S, Wree A, Guthoff RF, Stachs O, Langner S. Magnetic Resonance Microscopy of the Accommodative Apparatus. Klin Monbl Augenheilkd 2016;233:1320-3.
36. Weeber HA, Eckert G, Pechhold W, van der Heijde RG. Stiffness gradient in the crystalline lens. Graefes Arch Clin Exp Ophthalmol 2007;245:1357-66.
37. de Gracia P. Optical properties of monovision corrections using multifocal designs for near vision. J Cataract Refract Surg 2016;42:1501-10.
38. Schachar RA. Dynamic aspects of accommodation: age and presbyopia. Vision Res 2004;44:2313; author reply 2315-6.
39. Schachar RA, Chan RW, Fu M. Viscoelastic properties of fresh human lenses under 40 years of age: implications for the aetiology of presbyopia. Br J Ophthalmol 2011;95:1010-3.
40. Evans BJ. Monovision: a review. Ophthalmic Physiol Opt 2007;27:417-39.
41. Artigas Verde JM, Felipe Marcet A, Navea A, Fandino A, Artigas C, Diez-Ajenjo A. Age-induced change in the color of the human crystalline lens. Acta Ophthalmologica 2011. doi: 10.1111/j.1755-3768.2011.468.x.
42. Glasser A. Restoration of accommodation: surgical options for correction of presbyopia. Clin Exp Optom 2008;91:279-95.
43. Richdale K, Sinnott LT, Bullimore MA, Wassenaar PA, Schmalbrock P, Kao CY, Patz S, Mutti DO, Glasser A, Zadnik K. Quantification of age-related and per diopter accommodative changes of the lens and ciliary muscle in the emmetropic human eye. Invest Ophthalmol Vis Sci 2013;54:1095-105.
44. Rosen AM, Denham DB, Fernandez V, Borja D, Ho A, Manns F, Parel JM, Augusteyn RC. In vitro dimensions and curvatures of human lenses. Vision Res 2006;46:1002-9.
45. Atchison DA, Markwell EL, Kasthurirangan S, Pope JM, Smith G, Swann PG. Age-related changes in optical and biometric characteristics of emmetropic eyes. J Vis 2008;8:29.1-0.
46. Kasthurirangan S, Markwell EL, Atchison DA, Pope JM. In vivo study of changes in refractive index distribution in the human crystalline lens with age and accommodation. Invest Ophthalmol Vis Sci 2008;49:2531-40.
47. Weeber HA, van der Heijde RG. On the relationship between lens stiffness and accommodative amplitude. Exp Eye Res 2007;85:602-7.
48. Wu C, Han Z, Wang S, Li J, Singh M, Liu CH, Aglyamov S, Emelianov S, Manns F, Larin KV. Assessing age-related changes in the biomechanical properties of rabbit lens using a coaligned ultrasound and optical coherence elastography system. Invest Ophthalmol Vis Sci 2015;56:1292-300.
49. Jones CE, Atchison DA, Pope JM. Changes in lens dimensions and refractive index with age and accommodation. Optom Vis Sci 2007;84:990-5.
50. Langner S, Krueger PC, Lindner T, Niendorf T, Stachs O. In vivo MR microscopy of the human eye. Klin Monbl Augenheilkd 2014;231:1016-22.
51. Babizhayev MA, Nikolayev GN, Goryachev SN, Bours J. NMR spin-echo studies of hydration properties of the molecular chaperone alpha-crystallin in the bovine lens. Biochim Biophys Acta 2002;1598:46-54.
52. Vaghefi E, Pontre BP, Jacobs MD, Donaldson PJ. Visualizing ocular lens fluid dynamics using MRI: manipulation of steady state water content and water fluxes. Am J Physiol Regul Integr Comp Physiol 2011;301:R335-42.
53. Yilmaz A, Ulak FS, Batun MS. Proton T1 and T2 relaxivities of serum proteins. Magn Reson Imaging 2004;22:683-8.
54. Pescosolido N, Barbato A, Giannotti R, Komaiha C, Lenarduzzi F. Age-related changes in the kinetics of human lenses: prevention of the cataract. Int J Ophthalmol 2016;9:1506-17.
55. Wu JC, Wong EC, Arrindell EL, Simons KB, Jesmanowicz A, Hyde JS. In vivo determination of the anisotropic diffusion of water and the T1 and T2 times in the rabbit lens by high-resolution magnetic resonance imaging. Invest Ophthalmol Vis Sci 1993;34:2151-8.
56. Fornasa F. Diffusion-weighted Magnetic Resonance Imaging: What Makes Water Run Fast or Slow? J Clin Imaging Sci 2011;1:27.
57. Moffat BA, Landman KA, Truscott RJ, Sweeney MH, Pope JM. Age-related changes in the kinetics of water transport in normal human lenses. Exp Eye Res 1999;69:663-9.
58. Vaghefi E, Donaldson PJ. The lens internal microcirculation system delivers solutes to the lens core faster than would be predicted by passive diffusion. Am J Physiol Regul Integr Comp Physiol 2018;315:R994-R1002.
59. Mathias RT, Kistler J, Donaldson P. The lens circulation. J Membr Biol 2007;216:1-16.
60. Mathias RT, Rae JL, Baldo GJ. Physiological properties of the normal lens. Physiol Rev 1997;77:21-50.
61. Mathias RT, White TW, Gong X. Lens gap junctions

in growth, differentiation, and homeostasis. Physiol Rev 2010;90:179-206.
62. Zampighi GA, Simon SA, Hall JE. The Specialized Junctions of the Lens. In: Jeon KW, Friedlander M, editors. International Review of Cytology. New York: Academic Press, 1992:185-225.
63. Vaghefi E, Kim A, Donaldson PJ. Active Maintenance of the Gradient of Refractive Index Is Required to Sustain the Optical Properties of the Lens. Invest Ophthalmol Vis Sci 2015;56:7195-208.

Cite this article as: Stahnke T, Lindner T, Guthoff R, Stachs O, Wree A, Langner S, Niendorf T, Grabow N, Glass Ä, Beller E, Polei S. Ultrahigh field MRI determination of water diffusion rates in *ex vivo* human lenses of different age. Quant Imaging Med Surg 2021;11(7):3029-3041. doi: 10.21037/qims-20-1124

